PHOTONICS Research

Resonant transparency of a planar anapole metamaterial at terahertz frequencies

Xiangjun Li, Jie Yin, Jianjun Liu, Fangzhou Shu, Tingting Lang, Xufeng Jing, and Zhi Hong*

Centre for THz Research, China Jiliang University, Hangzhou 310018, China
**Corresponding author: hongzhi@cjlu.edu.cn*

Received 23 October 2020; revised 7 December 2020; accepted 7 December 2020; posted 8 December 2020 (Doc. ID 413361); published 21 January 2021

Anapole metamaterials have attracted growing attention in recent years due to their unique nonradiating and nontrivial properties. Although anapole modes have been demonstrated in metamaterials with three-dimensional structures, the design and realization of planar anapole metamaterials in a wide frequency range is still a big challenge. Here we propose and experimentally demonstrate a planar anapole metamaterial consisting of dumbbell-shaped apertures on a stainless-steel sheet at terahertz frequencies. The planar metamaterial can generate a resonant transparency in the terahertz spectrum due to the excitation of the anapole mode. Particularly, the frequency of anapole-induced resonant transparency can be tuned easily in the range of 0.15–0.93 THz by simply varying one geometric parameter of the dumbbell apertures. We anticipate that the resonant transparency in planar anapole metamaterials can be potentially used in filters, sensors, or other photonic devices.

https://doi.org/10.1364/PRJ.413361

1. INTRODUCTION

Metamaterials (MMs) have attracted considerable interest owing to their exotic electromagnetic properties and functionalities that do not exist in naturally occurring materials [1–5]. The desired electromagnetic response in MMs can be achieved by properly tailoring their meta-atoms or molecules by a few key multipole excitations, such as electric and magnetic dipoles. Recently, toroidal multipoles have attracted great attention because they are necessary for the complete multipole representation of an arbitrary radiating source along with the familiar electric and magnetic multipoles [6,7]. The toroidal dipole response in artificial MMs is usually weak and masked by more dominant electric and magnetic multipoles. Therefore, toroidal MMs are initially designed to amplify toroidal moments and suppress the competing electric and magnetic multipoles [8,9]. Fortunately, since the first experimental demonstration of toroidal dipole response in MMs in 2010 [10], there has been great progress in metallic or dielectric metamaterials from the microwave to visible wavelengths [11–18]. Toroidal dipoles offer a deeper insight into the multipolar response of subwavelength optical structures to many optical phenomena such as electromagnetically induced transparency (EIT) [16,19], unconventional optical activity [9,20], negative index of refraction [21], and bound states in the continuum (BIC) [22–25].

Recently, the anapole mode as a radiationless state with nontrivial oscillating current configuration has gained widespread attention, and it can be achieved by the destructive interference between the electrical and toroidal dipoles [26–30]. The nonradiating response of the anapole mode accompanied by enhanced near fields in single nanoparticles has found numerous applications such as in cloaking [31–33], harmonic generation [34–36], nanoscale lasers [37], and Raman scattering enhancement [38]. The anapole mode was first proposed and experimentally demonstrated in microwaves using metallic MMs with three-dimensional (3D) dumbbell apertures in 2013 [39]. By adjusting the quantity and rotation angle of metallic plates, anapole resonant electromagnetic transparency with a high Q factor was achieved. Recently, a quasiplanar plasmonic MM [40] from a combination of dumbbell apertures and vertical split-ring resonators (SRRs) was designed and fabricated, which exhibited an anapole response in the near-infrared (IR) spectra. However, the fabrication of 3D or quasiplanar structures of MMs is complicated, especially for the visible and terahertz (THz) frequency ranges. Therefore, designing planar anapole metamaterials is expected for realistic applications. Although there are some works discussing the anapole excitation in planar metamaterials in the microwave [41], THz [42–45], and optics [46–49] frequency ranges, the anapole-induced resonant transparency has not been observed. In addition, the tunability of anapole frequency is poor in previous works, and the design and realization of anapole resonance over a wide frequency range remains challenging.

In this paper, we describe the quantitative and experimental demonstration of anapole-induced total resonant transparency

in a dumbbell apertured planar metamaterial at THz frequencies. The near-Lorentz transmission line of resonant electromagnetic transparency was achieved through destructive interference between the electric dipole and toroidal dipole as well as effective suppression of the magnetic quadrupole. By optimizing the structure parameters, robust anapole resonance with high transmittance was achieved over the frequency range of 0.15–0.93 THz by adjusting one geometric parameter. The proposed planar anapole metamaterials were fabricated on stainless-steel sheets using a laser micromachining technique, and the measured transmissions of the resonant transparency were in good agreement with the simulations.

2. STRUCTURE OF THE PLANAR ANAPOLE METAMATERIAL AND SIMULATIONS

A schematic of the designed stainless-steel metamaterial and its dumbbell aperture unit cell are shown in Figs. 1(a) and 1(b). The feature sizes of the metamaterial are radius of circular cuts R, separation between the centers of the circular cuts W, and width G; the thickness of the stainless-steel sheet t is 200 μm. The surrounding medium is air, and the lattice periods are fixed along the x and y directions with $P_x = 1000$ μm and $P_y = 500$ μm, respectively. Quantitative calculations were conducted using finite-difference time-domain (FDTD) simulation software. In FDTD simulations, the planar metamaterial made of a stainless-steel sheet (conductivity $\sigma = 1.4 \times 10^6$ S/m) is illuminated by a normal incident plane wave, which is polarized along the y axis. Periodic boundary conditions are used in both the x and y directions and perfectly matched layers are applied in the z direction.

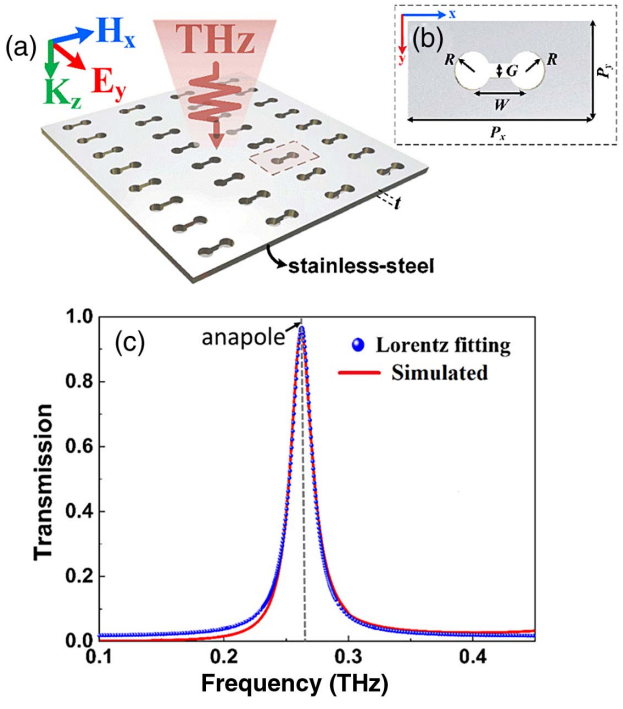

Fig. 1. (a), (b) Schematic of a planar anapole metamaterial with dumbbell-shaped apertures, which is illuminated by a normally incident plane wave with the electric field along the y axis. The structure parameters are radius R, width G, separation between the two circular cuts W, $P_x = 1{,}000$ μm, $P_y = 500$ μm, and the thickness of the stainless-steel sheet $t = 200$ μm. (c) Simulated and Lorentz fitted transmission resonance at 0.26 THz for the planar metamaterial when $R = 100$, $W = 300$, and $G = 75$ μm.

3. EXCITATION OF THE ANAPOLE RESONANCE

The transmission spectrum of the metamaterial was calculated in the frequency range 0.1–0.45 THz with $R = 100$ μm, $W = 300$ μm, and $G = 75$ μm as shown in Fig. 1(c). A Lorentz fitted resonance curve is also given. We can see a strong near Lorentz resonance located around 0.26 THz, the bandwidth of the resonance is ∼18 GHz (full width at half-maximum), and its peak transmission value is close to 1.0. To better understand the nature of the resonance, the corresponding distributions of the surface current, magnetic field, and electric field in the x-y, x-z, and x-y planes of the metamaterial at a frequency of 0.26 THz are illustrated in Figs. 2(a)–2(c), respectively. In Fig. 2(a), there is a pair of counter-rotating surface currents along the two circular cuts of the dumbbell aperture, which is induced by the y-polarized incidence; each can generate a magnetic field with the left circular cut along the $-z$ axis and the right cut for the $+z$ axis. The induced magnetic field patterns produce a circular head-to-tail magnetic moment (M), that is, toroidal dipole moment (T) along the y axis [see Fig. 2(b)] as well as a higher oscillating magnetic quadrupole (QM) [16,40]. Meanwhile, in Fig. 2(c), we can see that the induced electric dipole moment (P) along the y axis also contributes to the resonance. The excitations of T and P are more clearly seen in Fig. 2(d).

To further analyze the role of T and P in the observed resonance, Cartesian scattered powers for multipole moments were calculated based on the surface current in the metamaterial [50–52], as shown in Fig. 3(a), where P, M, T, QE, and QM are the five highest contributions of the electric dipole, magnetic dipole, toroidal dipole, electric quadrupole, and magnetic quadrupole, respectively; higher-order dipoles can be

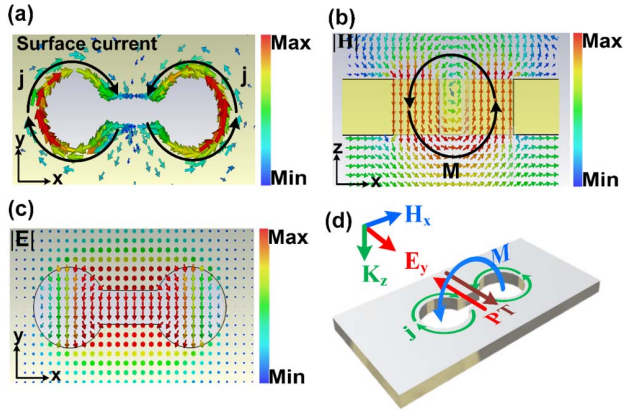

Fig. 2. (a) Surface current in the x-y plane, (b) magnetic field in the x-z plane, and (c) electric field in the x-y plane at the resonance of 0.26 THz for the planar metamaterial. The black arrows represent the direction of the surface current and magnetic field in (a) and (b), respectively. (d) Schematic of the excitation of toroidal dipole T and electric dipole P in the unit cell; M represents the head-to-tail magnetic moment, and j represents the surface current.

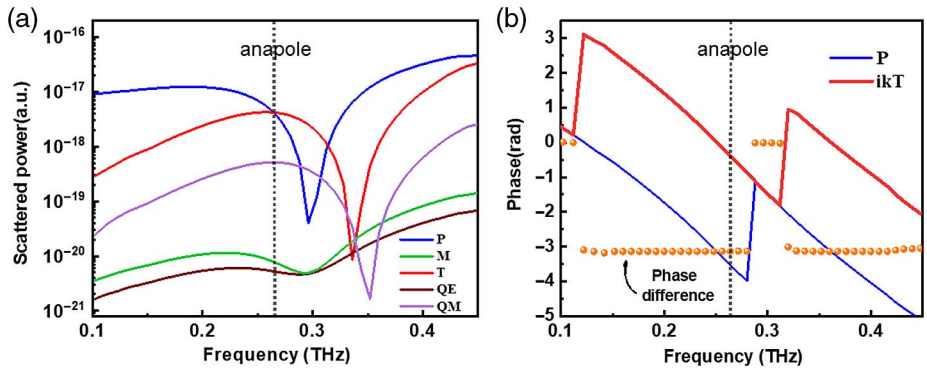

Fig. 3. (a) Five leading scattered powers of multipole decomposition for the planar metamaterial, where P, M, T, QE, and QM are electric dipole, magnetic dipole, toroidal dipole, electric quadrupole, and magnetic quadrupole, respectively. (b) Phase of Cartesian P and ikT. The orange dots represent the phase difference between them. The grey dotted line indicates the location of the corresponding resonant transparency at 0.26 THz.

ignored due to the extremely weak influence on the scattered intensity. It is clear that P and T show the two strongest scattered powers in the considered frequency range, meaning that the metamaterial is mainly excited by the electrical composition of the incident electromagnetic wave. Furthermore, P dominates the scattered powers at frequencies <0.26 and >0.32 THz, and T dominates between 0.26 and 0.32 THz. In particular, the scattered powers of P and T cross each other at 0.26 and 0.32 THz, respectively. The corresponding phase difference between P and ikT shown in Fig. 3(b) is zero at 0.32 THz, but π at 0.26 THz. Thus, destructive interference between P and ikT occurs only at 0.26 THz. In addition, the scattered power of the QM, which takes third place in the five leading multipoles at 0.26 THz, is only one-tenth that of the P, and other multipoles M and QE are 1/540 of the strength, indicating that the radiative losses of the multipoles other than P and T are greatly suppressed, leading to total resonant electromagnetic transparency or nonradiative anapole resonance (reflection is zero). We should mention here that the mechanism of resonant electromagnetic transparency is different from the Fano interference typically encountered in metamaterial systems, which mimics EIT. It exploits destructive interference between spatially and spectrally collocated and coherent oscillating induced electric and toroidal dipoles [39].

It is worth mentioning that an optical anapole was achieved in a 3D dumbbell-SRR metallic MM [40]. The destructive interference between P and ikT can occur when the MM is made of single dumbbell apertures without SRRs, but the scattered power of the QM is close to that of the P, which greatly increases the radiative loss of the resonance. In order to suppress the excitation of the QM, an SRR positioned vertically to the dumbbell aperture was introduced. As a result, the scattered power of the QM was reduced to approximately 1/3 of the P; however, the resonant transparency was not achieved, which may be due to the large material loss. For the simple dumbbell metamaterial we designed for the THz band, the scattered power of QM is effectively suppressed to only 1/10 of P, much smaller than that in the quasiplanar structure at the optical band, leading to the enhancement of anapole resonant transparency. This result can be explained by the large difference in the intrinsic ohmic resistance of metal at the optic and THz bands. As the ohmic resistance of the metal in the THz band is much smaller than that in the optic regime, the incident electric field induced pair of counter-rotating surface currents along the two circular cuts of the dumbbell aperture shown in Fig. 2 is greatly enlarged, resulting in the enhancement of the excitation of the T, i.e., relative suppression of the QM.

4. ANAPOLE RESONANCE IN A WIDE FREQUENCY RANGE

To obtain the characteristics of anapole resonance, we analyzed the influence of structural parameters of the dumbbell aperture on transmission resonance. Figures 4(a) and 4(b) illustrate the transmission spectra, scattered powers of T and P, and their phase differences at resonance for different values of R. The transmission resonance (including the resonance peak and frequency) is very sensitive to the parameter R; the resonance frequency decreases as R increases from 60 to 140 μm, and the resonance peak reaches its maximum when $R = 100$ μm. The scattered power of T at resonance decreases quickly and steadily as R increases, but P remains stable; at the same time, the phase difference between the P and ikT remains constant at π. Thus, partial destructive interference between P and ikT takes place over the entire range of R. In particular, the complete destructive interference leading to anapole-induced total resonant transparency appears only when $R = 100$ μm, which explains the variation in the resonance peak in Fig. 4(a).

Figures 4(c) and 4(d) plot the transmission spectra and scattered powers for the metamaterial at select values of W, which are similar to the results shown for select R values. As W increases from 200 to 300 μm, the transmission peak of the resonance increases quickly and reaches a maximum when anapole resonance is achieved at $W = 300$ μm, while the resonance frequency decreases steadily.

However, the resonance characteristics of the metamaterial with respect to G are quite different when R and W are fixed at 100 and 300 μm. As shown in Figs. 4(e) and 4(f), the resonance frequency shifts from 0.15 to 0.31 THz when G increases from 15 to 150 μm, but the resonance peak remains higher than 0.95. It is interesting to note that P and ikT

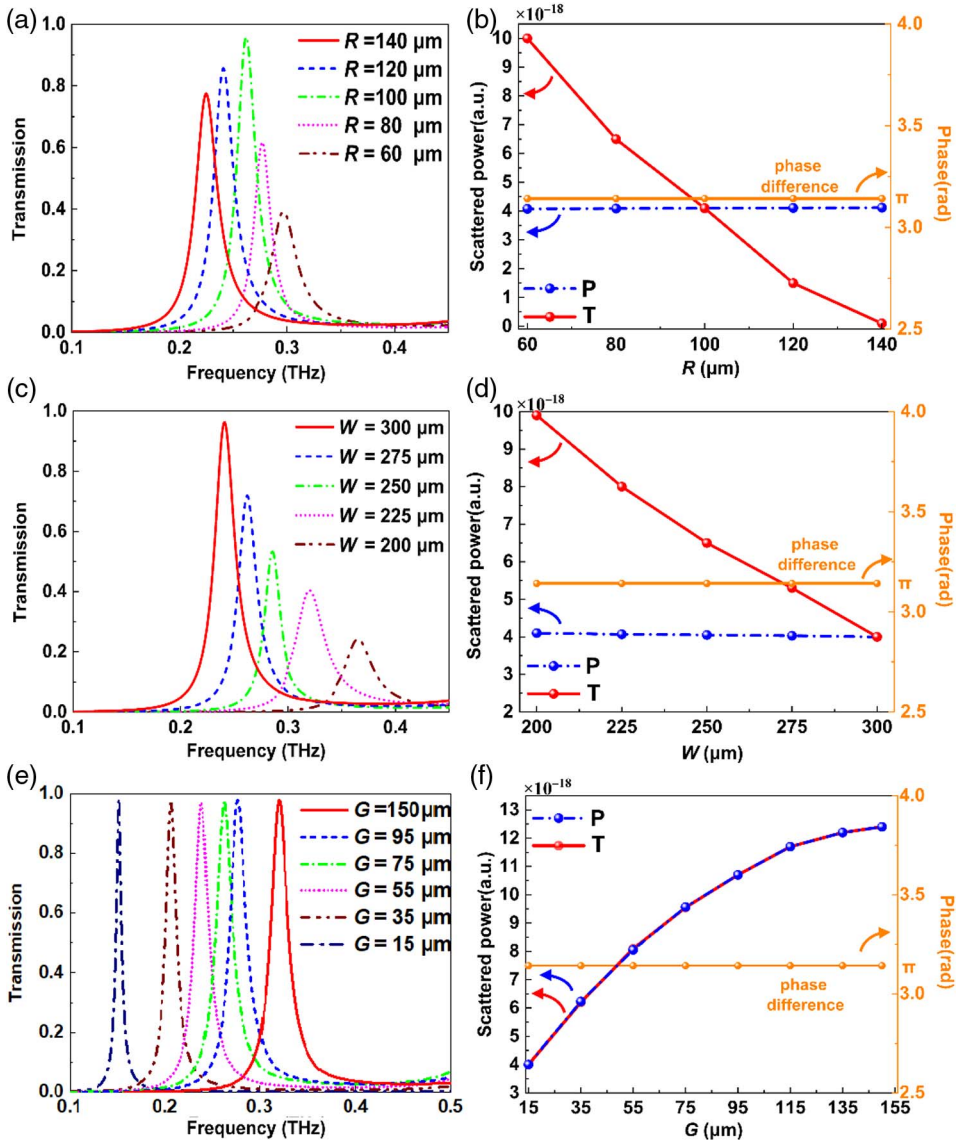

Fig. 4. Transmission spectra of planar metamaterials and corresponding scattered powers of the T and P at resonance (a), (b) with respect to R when $W = 300$ μm and $G = 75$ μm; (c), (d) with respect to W, when $R = 100$ μm and $G = 75$ μm; and (e), (f) with respect to G, when $R = 100$ μm and $W = 300$ μm. The phase difference between P and ikT remains constant at π.

not only increase quickly with the increase of G but also remain equal in strength and opposite in phase at all times [see Fig. 4(f)]; hence, complete destructive interference occurs in the entire G range, leading to anapole-induced total resonant transparency. That is, the anapole-induced resonant transparency can be tuned in the range of 0.15–0.31 THz by simply changing the width of the dumbbell aperture G.

Finally, a very simple way to enlarge the frequency range of the anapole resonance was identified, and the parameters are listed in Table 1. There are three anapole resonance bands achieved, namely, band A, band B, and band C, which span the frequency range of 0.15–0.93 THz. Band A covers the anapole resonance frequency range of 0.15–0.31 THz, which is discussed above. To double the anapole resonance frequency from band A to band B, reduce all three geometric parameters R, W, and G by dividing by 2. Similarly, to triple the anapole resonance frequency from band A to band C, reduce R, W, and G by dividing by 3. Figure 5 shows the anapole resonances in bands A, B, and C achieved by changing parameter G when the other two parameters R and W are fixed. It is noted that the transmission peak of the anapole resonance remains higher, over 0.90 and 0.85 in band B and in band C, respectively, but reduces sharply at frequencies higher than 1.0 THz when

Table 1. Three Anapole Resonance Bands with Different Structural Parameters

	Anapole Range (THz)	W (μm)	R (μm)	G (μm)
Band A	0.15–0.31	300	100	15–150
Band B	0.30–0.62	150	50	7.5–75
Band C	0.45–0.93	100	33	5–50

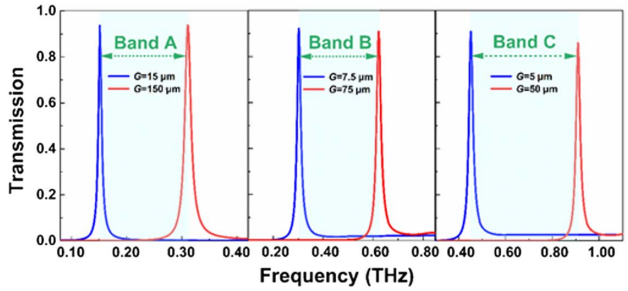

Fig. 5. Three anapole resonance bands produced by varying G when R and W are fixed. In the case of band A: $W = 300$ μm and $R = 100$ μm; band B: $W = 150$ μm and $R = 50$ μm; and band C: $W = 100$ μm and $R = 33$ μm.

parameters R, W, and G of the MM are reduced by a factor of 4 (not shown in the figure).

5. EXPERIMENTAL RESULTS

In order to confirm the previous simulated results, we fabricated the planar anapole metamaterials on a 200 μm thick stainless-steel sheet using a laser micromachining technique. The microscopic image of a fabricated sample is shown in the inset of Fig. 6. The transmission spectra of four samples with different widths G were measured using terahertz time-domain spectroscopy (THz-TDS) with a 70 dB dynamic range and 10 GHz spectral resolution. Figure 6 shows the simulated and measured transmissions of the four metamaterials for G values of 33, 54, 78, and 95 μm, respectively, where R and W are fixed as 100 μm and 300 μm, respectively. From Fig. 6, four strong anapole-induced resonant transparencies corresponding to four different G values were excited in the frequency range of band A as expected; the measured transmission peaks of the resonances were ~0.8. The measured transmission results were in good agreement with the simulations, and the small discrepancy is attributed to the low spectral resolution of the measurement system and imperfections of the fabrications. The anapole metamaterials in bands B and C are not experimentally shown because of the limited fabrication accuracy of the laser micromachining equipment.

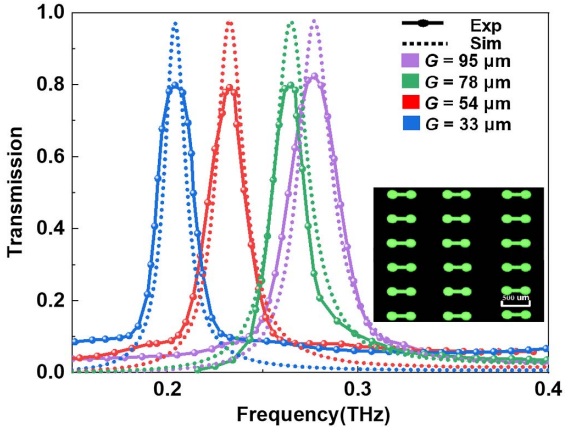

Fig. 6. Measured (solid line) and simulated (dotted line) transmission spectra of four anapole metamaterials with different values of $G = 33$, 54, 78, and 95 μm, respectively. Inset: microscopic top view of a fabricated planar anapole metamaterial with $R = 100$ μm, $W = 300$ μm, and $G = 78$ μm.

6. CONCLUSION

In conclusion, we quantitatively and experimentally demonstrated the total resonant transparency in a planar anapole metamaterial. The metamaterial consists of dumbbell apertures on a stainless-steel sheet, which was easily fabricated using a laser micromachining technique. The near-Lorentz transmission line of resonant electromagnetic transparency was achieved by destructive interference between the electric dipole and the toroidal dipole, with concurrent suppression of the magnetic quadrupole. Thus, a simple method for achieving robust anapole-induced resonant transparency with high transmittance in the frequency range of 0.15–0.93 THz is provided. The measured transmission results were in good agreement with the simulations. Such planar anapole metamaterials with low ohmic loss at THz frequencies can be potentially used in filters, sensors, or other photonic devices.

Funding. National Natural Science Foundation of China (61875179, 61875251, 12004362); Primary Research and Development Plan of Zhejiang Province (2019C03114).

Disclosures. The authors declare no conflicts of interest.

REFERENCES

1. R. A. Shelby, D. R. Smith, and S. Schultz, "Experimental verification of a negative index of refraction," Science **292**, 77–79 (2001).
2. T. J. Yen, W. J. Padilla, N. Fang, D. C. Vier, D. R. Smith, J. B. Pendry, D. N. Basov, and X. Zhang, "Terahertz magnetic response from artificial materials," Science **303**, 1494–1496 (2004).
3. D. Schurig, J. J. Mock, B. J. Justice, S. A. Cummer, J. B. Pendry, A. F. Starr, and D. R. Smith, "Metamaterial electromagnetic cloak at microwave frequencies," Science **314**, 977–980 (2006).
4. M. Khorasaninejad, W. T. Chen, R. C. Devlin, J. Oh, A. Y. Zhu, and F. Capasso, "Metalenses at visible wavelengths: diffraction-limited focusing and subwavelength resolution imaging," Science **352**, 1190–1194 (2016).
5. N. I. Zheludev and Y. S. Kivshar, "From metamaterials to metadevices," Nat. Mater. **11**, 917–924 (2012).
6. V. M. Dubovik and V. V. Tugushev, "Toroid moments in electrodynamics and solid-state physics," Phys. Rep. **187**, 145–202 (1990).
7. I. B. Zel'Dovich, "The relation between decay asymmetry and dipole moment of elementary particles," Sov. Phys. JETP **6**, 1148–1155 (1958).
8. N. Talebia, S. Guoa, and P. A. van Aken, "Theory and applications of toroidal moments in electrodynamics: their emergence, characteristics, and technological relevance," Nanophotonics **7**, 93–110 (2018).
9. N. Papasimakis, V. A. Fedotov, V. Savinov, T. A. Raybould, and N. I. Zheludev, "Electromagnetic toroidal excitations in matter and free space," Nat. Mater. **15**, 263–271 (2016).
10. T. Kaelberer, V. A. Fedotov, N. Papasimakis, D. P. Tsai, and N. I. Zheludev, "Toroidal dipolar response in a metamaterial," Science **330**, 1510–1512 (2010).
11. Z. Dong, P. Ni, J. Zhu, X. Yin, and X. Zhang, "Toroidal dipole response in a multifold double-ring metamaterial," Opt. Express **20**, 13065–13070 (2012).
12. T. A. Raybould, V. A. Fedotov, N. Papasimakis, I. Kuprov, I. J. Youngs, W. T. Chen, D. P. Tsai, and N. I. Zheludev, "Toroidal circular dichroism," Phys. Rev. B **94**, 035119 (2016).

13. Y. Fan, Z. Wei, H. Li, H. Chen, and C. M. Soukoulis, "Low-loss and high-Q planar metamaterial with toroidal moment," Phys. Rev. B **87**, 115417 (2013).
14. L. Cong, Y. K. Srivastava, and R. Singh, "Tailoring the multipoles in THz toroidal metamaterials," Appl. Phys. Lett. **111**, 081108 (2017).
15. M. Gupta, V. Savinov, N. Xu, L. Cong, G. Dayal, S. Wang, W. Zhang, N. I. Zheludev, and R. Singh, "Sharp toroidal resonances in planar terahertz metasurfaces," Adv. Mater. **28**, 8206–8211 (2016).
16. B. Han, X. Li, C. Sui, J. Diao, X. Jing, and Z. Hong, "Analog of electromagnetically induced transparency in an E-shaped all-dielectric metasurface based on toroidal dipolar response," Opt. Mater. Express **8**, 2197–2207 (2018).
17. Y. W. Huang, W. T. Chen, P. C. Wu, V. A. Fedotov, V. Savino, Y. Z. Ho, Y. F. Chau, N. I. Zheludev, and D. P. Tsai, "Design of plasmonic toroidal metamaterials at optical frequencies," Opt. Express **20**, 1760–1768 (2012).
18. B. Oeguet, N. Talebi, R. Vogelgesang, W. Sigle, and P. A. van Aken, "Toroidal plasmonic eigenmodes in oligomer nanocavities for the visible," Nano Lett. **12**, 5239–5244 (2012).
19. F. Y. He, B. X. Han, X. J. Li, T. T. Lang, X. F. Jing, and Z. Hong, "Analogue of electromagnetically induced transparency with high-Q factor in metal-dielectric metamaterials based on bright-bright mode coupling," Opt. Express **27**, 37590–37600 (2019).
20. L. Guo, M. Li, X. Huang, and H. Yang, "Electric toroidal metamaterial for resonant transparency and circular cross-polarization conversion," Appl. Phys. Lett. **105**, 033507 (2014).
21. K. Marinov, A. D. Boardman, V. A. Fedotov, and N. I. Zheludev, "Toroidal metamaterial," New J. Phys. **9**, 324 (2007).
22. Y. He, G. T. Guo, T. H. Feng, Y. Xu, and A. E. Miroshnichenko, "Toroidal dipole bound states in the continuum," Phys. Rev. B **98**, 161112 (2018).
23. S. Han, L. Cong, Y. K. Srivastava, B. Qiang, M. V. Rybin, A. Kumar, R. Jain, W. X. Lim, V. G. Achanta, S. S. Prabhu, Q. J. Wang, Y. S. Kivshar, and R. Singh, "All-dielectric active terahertz photonics driven by bound states in the continuum," Adv. Mater. **31**, 1901921 (2019).
24. X. F. Wang, S. Y. Li, and C. B. Zhou, "Polarization-independent toroidal dipole resonances driven by symmetry-protected BIC in ultraviolet region," Opt. Express **28**, 11983–11989 (2020).
25. X. Luo, X. J. Li, T. T. Lang, X. F. Jing, and Z. Hong, "Excitation of high Q toroidal dipole resonance in an all-dielectric metasurface," Opt. Mater. Express **10**, 358–368 (2020).
26. K. V. Baryshnikova, D. A. Smirnova, B. S. Luk'Yanchuk, and Y. S. Kivshar, "Optical anapoles: concepts and applications," Adv. Opt. Mater. **7**, 1801350 (2019).
27. A. E. Miroshnichenko, A. B. Evlyukhin, Y. F. Yu, R. M. Bakker, A. Chipouline, A. I. Kuznetsov, B. S. Luk'Yanchuk, B. N. Chichkov, and Y. S. Kivshar, "Nonradiating anapole modes in dielectric nanoparticles," Nat. Commun. **6**, 8069 (2015).
28. V. Savinov, N. Papasimakis, D. P. Tsai, and N. I. Zheludev, "Optical anapoles," Commun. Phys. **2**, 69 (2019).
29. E. A. Gurvitz, K. S. Ladutenko, P. A. Dergachev, A. B. Evlyukhin, A. E. Miroshnichenko, and A. S. Shalin, "The high-order toroidal moments and anapole states in all-dielectric photonics," Laser Photon. Rev. **13**, 1800266 (2019).
30. N. A. Nemkov, A. A. Basharin, and V. A. Fedotov, "Electromagnetic sources beyond common multipoles," Phys. Rev. A **98**, 023858 (2018).
31. L. Wei, Z. Xi, N. Bhattacharya, and H. P. Urbach, "Excitation of the radiationless anapole mode," Optica **3**, 799–802 (2016).
32. W. Liu, J. Zhang, B. Lei, H. Hu, and A. E. Miroshnichenko, "Invisible nanowires with interfering electric and toroidal dipoles," Opt. Lett. **40**, 2293–2296 (2015).
33. A. K. Ospanova, G. Labate, L. Matekovits, and A. A. Basharin, "Multipolar passive cloaking by nonradiating anapole excitation," Sci. Rep. **8**, 12514 (2018).
34. G. Grinblat, Y. Li, M. P. Nielsen, R. F. Oulton, and S. A. Maier, "Efficient third harmonic generation and nonlinear subwavelength imaging at a higher-order anapole mode in a single germanium nanodisk," ACS Nano **11**, 953–960 (2017).
35. T. Shibanuma, G. Grinblat, P. Albella, and S. A. Maier, "Efficient third harmonic generation from metal-dielectric hybrid nanoantennas," Nano Lett. **17**, 2647–2651 (2017).
36. V. F. Gili, L. Ghirardini, D. Rocco, G. Marino, I. Favero, I. Roland, G. Pellegrini, L. Duo, M. Finazzi, L. Carletti, A. Locatelli, A. Lemaitre, D. Neshev, C. D. Angelis, G. Leo, and M. Celebrano, "Metal-dielectric hybrid nanoantennas for efficient frequency conversion at the anapole mode," Beilstein J. Nanotech. **9**, 2306–2314 (2018).
37. J. S. T. Gongora, A. E. Miroshnichenko, Y. S. Kivshar, and A. Fratalocchi, "Anapole nanolasers for mode-locking and ultrafast pulse generation," Nat. Commun. **8**, 15535 (2017).
38. D. G. Baranov, R. Verre, P. Karpinski, and M. Käll, "Anapole-enhanced intrinsic Raman scattered from silicon nanodisks," ACS Photon. **5**, 2730–2736 (2018).
39. V. A. Fedotov, A. V. Rogacheva, V. Savinov, D. P. Tsai, and N. I. Zheludev, "Resonant transparency and non-trivial non-radiating excitations in toroidal metamaterials," Sci. Rep. **3**, 2967 (2013).
40. P. C. Wu, C. Y. Liao, V. Savinov, T. L. Chung, W. T. Chen, Y. W. Huang, P. R. Wu, Y. H. Chen, A. Q. Liu, N. I. Zheludev, and D. P. Tsai, "Optical anapole metamaterial," ACS Nano **12**, 1920–1927 (2018).
41. A. A. Basharin, V. Chuguevsky, N. Volsky, M. Kafesaki, and E. N. Economou, "Extremely high Q-factor metamaterials due to anapole excitation," Phys. Rev. B **95**, 035104 (2017).
42. S. Han, M. Gupta, L. Cong, Y. K. Srivastava, and R. Singh, "Toroidal and magnetic Fano resonances in planar THz metamaterials," J. Appl. Phys. **122**, 113105 (2017).
43. M. Gupta and R. Singh, "Toroidal versus Fano resonances in high Q planar THz metamaterials," Adv. Opt. Mater. **4**, 2119–2125 (2016).
44. X. Liu, Z. Liu, M. Hua, L. Wang, and F. Yang, "Tunable terahertz metamaterials based on anapole excitation with graphene for reconfigurable sensors," ACS Appl. Nano Mater. **3**, 2129–2133 (2020).
45. M. V. Cojocari, K. I. Schegoleva, and A. A. Basharin, "Blueshift and phase tunability in planar THz metamaterials: the role of losses and toroidal dipole contribution," Opt. Lett. **42**, 1700–1703 (2017).
46. A. K. Ospanova, I. V. Stenishchev, and A. A. Basharin, "Anapole mode sustaining silicon metamaterials in visible spectral range," Laser Photon. Rev. **12**, 1800005 (2018).
47. S. Liu, Z. Wang, W. Wang, J. Chen, and Z. Chen, "High Q-factor with the excitation of anapole modes in dielectric split nanodisk arrays," Opt. Express **25**, 22375–22387 (2017).
48. J. F. Algorri, D. C. Zografopoulos, A. Ferraro, B. G. Camara, R. Beccherelli, and J. M. Sanchez-Pena, "Ultrahigh-quality factor resonant dielectric metasurfaces based on hollow nanocuboids," Opt. Express **27**, 6320–6330 (2019).
49. R. Wang and L. Dal Negro, "Engineering non-radiative anapole modes for broadband absorption enhancement of light," Opt. Express **24**, 19048–19062 (2016).
50. V. Savinov, V. A. Fedotov, and N. I. Zheludev, "Toroidal dipolar excitation and macroscopic electromagnetic properties of metamaterials," Phys. Rev. B **89**, 205112 (2014).
51. A. A. Basharin, M. Kafesaki, E. N. Economou, C. M. Soukoulis, V. A. Fedotov, V. Savinov, and N. I. Zheludev, "Dielectric metamaterials with toroidal dipolar response," Phys. Rev. X **5**, 011036 (2015).
52. E. E. Radescu and G. Vaman, "Exact calculation of the angular momentum loss, recoil force, and radiation intensity for an arbitrary source in terms of electric, magnetic, and toroid multipoles," Phys. Rev. E **65**, 046609 (2002).